REVISTA MATÉRIA
V.23 N.02
ISSN 1517-7076 artigo e-12043, 2018

Study of the martensitic transition in Ni-Mn-Sn-Ti ferromagnetic shape memory alloys

Federico Guillermo Bonifacich[1], Osvaldo Agustín Lambri[1], José Ignacio Pérez-Landazábal [2,3],Vicente Recarte[2,3], Damián Gargicevich[1], Griselda Irene Zelada[1], Ricardo Raúl Mocellini[1],Vicente Sánchez-Alarcos[2,3], Aldo Marenzana[4], Fernando Plazaola[5]

[1] CONICET-UNR-Laboratorio de Materiales, Escuela de Ingeniería Eléctrica, Centro de Tecnología e Investigación Eléctrica, Facultad de Ciencias Exactas, Ingeniería y Agrimensura, Av. Pellegrini 250, CP: 2000, Rosario, Santa Fe, Argentina.
e-mail: bonifaci@fceia.unr.edu.ar; olambri@fceia.unr.edu.ar; gargi@fceia.unr.edu.ar; gizelada@fceia.unr.edu.ar
[2] Departamento de Física, Universidad Pública de Navarra, Campus de Arrosadía 31006, Pamplona, Navarra, Spain.
[3] Institute for Advanced Materials (INAMAT), Universidad Pública de Navarra,Campus de Arrosadía 31006, Pamplona, Navarra, Spain.
e-mail: ipzlanda@unavarra.es; recarte@unavarra.es; vicente.sanchez@unavarra.es
[4] Instituto de Física Rosario-CONICET, Avda. 27 de Febrero 210 bis, CP: 2000 Rosario, Santa Fe, Argentina.
[5] Elektrika eta Elektronika Saila, Zientzia eta Teknologia Fakultatea, Euskal Herriko Unibertsitatea, P.K. 644, 48080 Bilbao, Biscaia, Spain.
e-mail: fernando.plazaola@ehu.eus

ABSTRACT

In the present work, mechanical spectroscopy measurements as a function of temperature and strain have been performed in (at.%) $Ni_{50}Mn_{37}Sn_{13-x}Ti_x$ (x=0, 0.5 and 2) ferromagnetic shape memory alloys in order both to study martensitic transition phenomenon and also to determine its temperature of appearance. For mechanical spectroscopy measurements, a five elements piezoelectric device recently developed has been used. In addition, other characterization techniques as, differential thermal analysis and superconducting quantum interference magnetic spectroscopy, were also used. Besides, relaxation processes near the martensitic transition temperature have been also observed.

Keywords: NiMnSn, ferromagnetic shape memory alloys, composite piezoelectric oscillator, short and brittle samples.

1. INTRODUCTION

Ni–Mn–X (X = Ga, In, Sn, Sb) alloys are currently attracting considerable attention due to the peculiar multifunctional properties that show as a result of coupling between structure and magnetism (namely giant magnetoresistance, magnetic shape memory effect or large magnetocaloric effect) [1-3]. In particular, these properties are linked to modification of the magnetic characteristics of the alloy as a consequence of the occurrence of a first-order martensitic transformation (MT) between magnetically ordered phases. In Ni–Mn–Ga alloys the MT takes place from ferromagnetic austenite to a ferromagnetic martensite showing higher saturation magnetization [4]. In contrast, in Ni–Mn–Z alloys (Z = In, Sn, Sb) the ferromagnetism of the austenite vanishes at the MT, concurrently with the appearance of antiferromagnetic correlations, thus resulting in a martensitic phase with lower magnetic moment [5-7]. In this latter case, the metamagnetic character of the MT gives rise to new interesting phenomena, such as: the magnetic-field induction of the MT, the kinetic arrest of the martensite, the exchange bias or the observation of a peculiar isothermal character in the MT. These phenomena have also been widely studied in recent years [8-11].

On the other hand, the motion of magnetic domains also depends on their interaction with structural defects [12]. In addition, in recent works, the influence of defects on the MT and the interaction between twin boundary and defects has been studied [13,14].

In the present work, mechanical spectroscopy measurements as a function of temperature and strain have been performed in (at.%) $Ni_{50}Mn_{37}Sn_{13-x}Ti_x$ (x=0, 0.5 and 2) ferromagnetic shape memory alloys in

Corresponding Author : Federico Guillermo Bonifacich Received on: 01/08/2017 Accepted on: 13/12/2017

10.1590/S1517-707620180002.0379

order both to study martensitic transition phenomenon and also to determine its temperature of appearance.

MS measurements as a function of temperature and strain were performed in a piezoelectric composite oscillator recently developed and assembled at the laboratory [15]. It should be highlighted that the here shown equipment is an important solution for measuring small and brittle samples, often involved in pilot development of new alloys, which cannot be matched in frequency. Other characterization techniques such as differential thermal analysis and superconducting quantum interference magnetic spectroscopy were also used in order to check the obtained results from MS.

2. THEORETICAL BACKGROUND FOR THE NEW PIEZOELECTRIC EQUIPMENT

The Marx-three component piezoelectric resonator requires that the lengths of the components are frequency-matched to their half-wavelengths [16]. In these conditions, both the displacement and the strain waves exhibit a continuous behaviour through the composite oscillator, and the condition of zero strain and maximum displacement is satisfied at the end of each element [16-18]. From the equivalent electrical circuit of the Marx three component oscillator, the well-known equations for frequency, f, and damping, Q^{-1}, have been obtained by Robinson [19] and Marx [16]

$$f_T^{\,2} m_T = f_1^{\,2} m_1 + f_2^{\,2} m_2 + f_3^{\,2} m_3 \tag{1}$$

$$Q_T^{-1} m_T = Q_1^{-1} m_1 + Q_2^{-1} m_2 + Q_3^{-1} m_3 \tag{2}$$

wherein, m_T, f_T and $Q^{-1}{}_T$, are the total mass (Σm_i), the oscillating frequency (resonant) and the damping of the whole oscillator, respectively. m_i, f_i and $Q^{-1}{}_i$ are the mass, frequency and damping corresponding to the element "*i*", respectively. *i*=1 to 3, correspond to crystal gauge, crystal driver and sample; respectively. As it can be easily inferred from equations (1) and (2) the squared frequency and damping of the whole oscillator are averaged values weighted by the total mass of their components [15-19].

On the other hand, the new composite oscillator here shown, involves a thin-flat driver, two spacer bars, a sample and crystal gauge assembled as shown in Figure 1. The spacer bars and sample are non-matched in half-wavelength. The driver is a thin-plate commercial piezoelectric quartz crystal. The gauge is a typical 18.5° *x* cut α-quartz crystal gold plated on z faces. The length and mass of the driver are not significant in comparison to the other elements and then, they can be neglected. So, the driver will be assumed as an elastic membrane which generates a plane wave front. This assumption allows considering at the interface, the displacement and strain, maximum and nil, respectively [15].

Since each element of the oscillator has not the same resonance frequency, equation (1) and (2) cannot be used. Nevertheless, the resonance frequency can be calculated by means equation (3) for the five elements composite oscillator, such that [15,20,21]

$$\frac{l_{sb1}}{\lambda_{sb1}/2} + \frac{l_s}{\lambda_s/2} + \frac{l_{sb2}}{\lambda_{sb2}/2} + \frac{l_{CG}}{\lambda_{CG}/2} = n \tag{3}$$

where the sub-indexes *sbi* (with *i* = 1, 2) are related to the spacer bars, *S* corresponds to the sample, *CG* is for the crystal gauge and *n* is an integer. Spacer bars #1 and #2, hereafter, will be referred to upper bar and lower bar, respectively, see Figure 1.

Thus, by assuming that the speed of sound in the spacer bars (for instance quartz or Pyrex) and the crystal gauge are known, the wavelength corresponding to the sample can be easily determined from equation (3). Then, the speed of sound in the sample can be obtained using $v = f \cdot \lambda$, where *f* is the frequency imposed by the driver. Finally, the elastic modulus is $E = \rho \cdot v^2$, ρ being the density of the sample [15,22].

As said before, equation (2) cannot be used because of the unmatched frequencies of the elements of the oscillator. In consequence, a more general expression must be used [15].

$$Q_T^{-1} W_T = Q_{sb1}^{-1} W_{sb1} + Q_S^{-1} W_S + Q_{sb2}^{-1} W_{sb2} + Q_{CG}^{-1} W_{CG} \tag{4}$$

wherein, W_T is the storage energy of the whole oscillator, and Q_S^{-1}, Q_{CG}^{-1}, Q_{sb1}^{-1}, Q_{sb2}^{-1} and Q_T^{-1} are the damping of the sample, the crystal gauge, the spacer bars (sb1 and sb2) and the total of whole oscillator, respectively. So, if the damping of each component is known, the damping of the sample from equation (4) can be calculated.

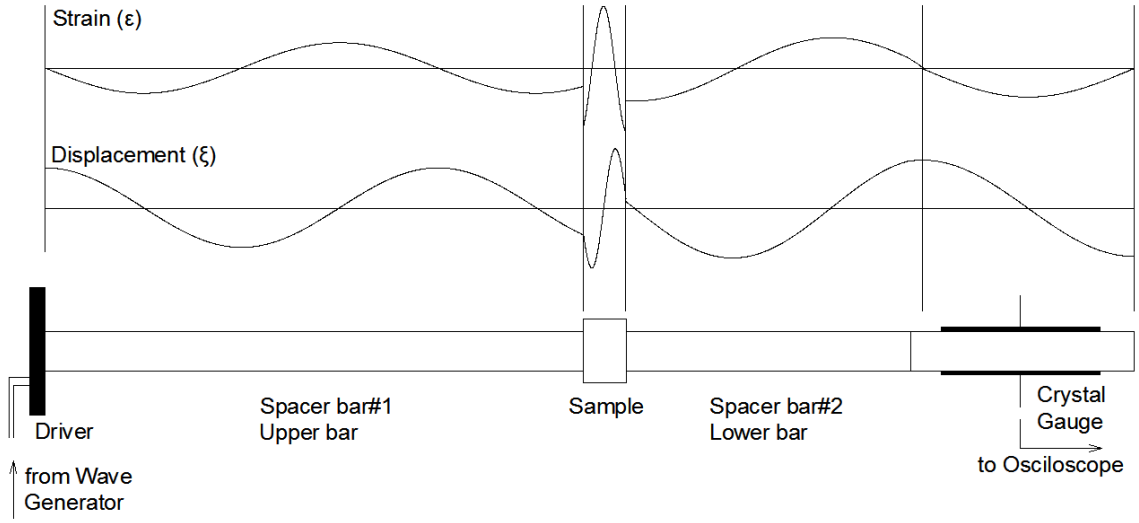

Figure 1: Five composite oscillator. The driver is a thin-flat power quartz crystal. The two spacer bars and the sample are out of the match in frequency. The crystal gauge is matched in frequency. Displacement wave, even continuous, exhibits peaked shape behaviour at the interface and then the strain is not continuous.

The stored energy in each element is [15]

$$W_i = \frac{1}{2} A_i E_i \varepsilon_{mi}^{\,2} \int_{l_{i-1}}^{l_{i-1}+l_i} \sin^2\left(\frac{2\pi}{\lambda_i} x - c_i\right) dx \tag{5}$$

where x is the position on the element from the origin and A_i, E_i, ε_{mi}, λ_i and c_i are the area, the elastic modulus, the maximum oscillating strain, the wavelength and the phase angle for the element "i", respectively.

In order to calculate the equation (5) for each element, it is necessary to obtain firstly the phase-constants, c_i, and subsequently ε_{mi}. The phase constants will be obtained from the displacements expressions. Strain expressions can be deduced easily from the derivative of the corresponding displacement, see Figure 1. Thus, by considering the origin of the coordinates system at the left end of the composite oscillator, the expressions for the displacement in each spacer bar and in the sample result [15],

$$\xi_{sb1}(x) = \xi_{sb1Max} \cos\left(\frac{2\pi}{\lambda_{sb1}} x\right) \tag{6}$$

$$\xi_S(x) = \xi_{SMax} \cos\left(\frac{2\pi}{\lambda_S} x - c_2\right) \tag{7}$$

$$\xi_{sb2}(x) = \xi_{sb2Max} \cos\left(\frac{2\pi}{\lambda_{sb1}} x - c_3\right) \tag{8}$$

By working mathematically, the constants c2 and c3 can be obtained, such that (see for more details Ref. [15])

$$c_2 = \frac{2\pi}{\lambda_S} l_{sb1} - tg^{-1}\left(\frac{E_{sb} A_{sb} \lambda_S}{E_S A_S \lambda_{sb}} tg\left(\frac{2\pi}{\lambda_{sb}} l_{sb1}\right)\right) \tag{9}$$

$$c_3 = \frac{2\pi}{\lambda_{sb}} \left(l_{sb1} + l_S + l_{sb2}\right) \tag{10}$$

Regarding the obtainment of ε_{mi} terms. As it was pointed out above, the displacement at the interface of two adjacent elements of the composite oscillator must be the same. Then, we can write for the spacer bar #1 and the sample;

$$\xi_{sb1}(l_{sb1}) = \xi_S(l_{sb1}) \tag{11}$$

By taking the derivative and working mathematically, we can write

$$\frac{\varepsilon_{sb1Max}}{\varepsilon_{SMax}} = \frac{\lambda_S}{\lambda_{sb}} \frac{\cos\left(\frac{2\pi}{\lambda_S} l_{sb1} - c_2\right)}{\cos\left(\frac{2\pi}{\lambda_{sb}} l_{sb1}\right)} \tag{12}$$

Likewise, for the interface between the spacer bar #2 and the sample, we can obtain

$$\frac{\varepsilon_{sb2Max}}{\varepsilon_{SMax}} = \frac{\lambda_S}{\lambda_{sb}} \frac{\cos\left(\frac{2\pi}{\lambda_S}(l_{sb1} + l_S) - c_2\right)}{\cos\left(\frac{2\pi}{\lambda_{sb}}(l_{sb1} + l_S) - c_3\right)} \tag{13}$$

Finally, the maximum strain in the spacer bar #2 can be obtained from the continuity condition of the strains between the crystal gauge (CG) and the bar, that is

$$\varepsilon_{sb2Max} = \varepsilon_{CGMax} \frac{\lambda_{CG}}{\lambda_{sb2}} \tag{14}$$

The maximum strain in the crystal gauge $\varepsilon_{CG\,Max}$ is given by the well-known expression [16]

$$\varepsilon_{CGMax} = V_e \frac{1}{f_c l_c} \sqrt{\frac{1}{2 m_c f_c R F_c}} = \beta V_g \tag{15}$$

where V_e is the excitation voltage, f_c is the resonant frequency, F_c is the damping of the oscillator and l_c, m_c and R are the length and mass of the crystal and the resistance of the equivalent circuit; respectively.

By knowing ε_{CGMax}, the strain values of ε_{sb2Max}, ε_{SMax} and ε_{sb1Max} can be obtained through equation (12) to (14). In addition, if the cross section, the modulus and the length of each component of the oscillator are known, the storage energies for the spacer bars (W_{sb1}, W_{sb2}), the sample (W_S) and the crystal gauge (W_{CG}) can be calculated from equation (5). See for more details Ref. [15].

3. MATERIALS AND METHODS

Polycrystalline ingots of nominal composition (at.%) $Ni_{50}Mn_{37}Sn_{13-x}Ti_x$ (x=0, 0.5 and 2), called hereafter Ti0, Ti05 and Ti2, respectively, were prepared from high-purity elements by arc melting under a protective Ar atmosphere. The addition of titanium is performed in order to refine the grain size. The ingots were remelted several times and then homogenized in vacuum quartz ampoules at 1273 K for 2 h. After homogenization, samples were annealed at 1173 K in ampoules under Ar for 30 min, followed by quenching in iced water. The composition of the elaborated alloys was analyzed by energy-dispersive spectroscopy in a JEOL JSM-5610LV scanning electron microscope. Samples were parallelepiped shape with dimensions 6.82 mm x 8.12 mm x 5.34 mm, 4.98 mm x 4.40 mm x 1.9 mm and 4.82 mm x 5.74 mm x 1.5 mm for Ti0, Ti05 and Ti2, respectively.

Samples were cemented to the oscillator components by using high alumina cement, as it is detailed in Ref. [15]. After the cementing process, the entire composite oscillator was placed into the vacuum chamber of the device in order to dry the cemented parts. The system was evacuated at a vacuum better than 90 mTorr during 72 hours at RT. Spacer bars were cylinders of fused quartz of 6 mm diameter and 160 mm and 140 mm length for the *sb1* and *sb2*, respectively.

For the damping measurement ($Q^{-1}{}_T$ in equation (4)) the usual expression for calculating the damping from the slope of the straight line which results from the least squares fitting of the natural logarithm of the decaying areas versus time was used [17,23],

$$\ln(A_n) = \ln(A_0) - \pi\, Q_T^{-1}\, n \tag{16}$$

where A_n is the area of the n^{th} decaying oscillation, A_0 is the initial area of the starting decaying oscillation and n is the period number, see Figure 2. For damping measurements the same initial and end values of the decaying areas were used for eliminating some possible distortion due to the appearance of amplitude dependent damping effects [23]. Once $Q^{-1}{}_T$ was measured, by coupling equations (4) to (15), the damping of the sample can be calculated.

The measurements were performed under a pure Ar protective atmosphere, and the heating rates employed in the tests were 1K/minute controlled by means of a PID (Novus N480D) temperature controller.

The ultrasonic wave was generated by a thin-flat power commercial piezoelectric quartz driver, produced by Apple Vista Technology Ltd. It was excited by a synthesized waveform generator Rigol DG 1022 plus a power amplifier of plane response with low harmonic distortion. The diameter, thickness and weight of the driver were 25 mm, 1 mm and 4.55 g, respectively. The crystal gauge (see Figure 1) was a quartz piezoelectric crystal of high quality factor manufactured by Bliley Electric Company. The dimensions of the crystal gauge were 5.00mm x 5.00mm x 56.10mm and a weight of 4.10g, with gold deposited faces. The decaying was finally recorded by a high-speed digital storage oscilloscope Rigol DS 1052 E. For data analysis the oscilloscope was connected to a personal computer.

The new piezoelectric equipment was also prepared for working in the amplitude dependent damping regime. As a consequence of measuring in free decay mode, the amplitude dependent damping (ADD) behaviour promoted by the appearance of non-linear effects (the double of stress does not lead to the double of strain) can be easily measured by taking the derivative of the decaying oscillations regarding the period number [23-26]. In fact, the damping as a function of the maximum strain on the sample, ε_0, was calculated from equation (17)

$$Q^{-1}{}_T(\varepsilon_0) = -\frac{1}{\pi}\frac{d(\ln(A_n))}{dn} \tag{17}$$

The decaying of the oscillations were performed at constant temperature (T ± 0.5 K). Polynomials were fitted to the curve of the decaying areas of the longitudinal vibrations as a function of the period number by means of Chi-square fitting. Subsequently the equation (17) was applied. Polynomials of degree higher than 1 indicate that Q_T^{-1} is a function of ε_0, leading to the appearance of ADD effects, as it can be inferred easily. This procedure allows obtaining the damping as a function of the maximum strain (ε_0) from free decaying oscillations [23-26].

Figure 2 shows the logarithm of the decaying oscillations as a function of the period number for the case of non linear effects. Upper inset shows the decaying oscillations recorder by the system and the lower inset shows the damping against ε0 obtained from equation (17).

Then, as said before, by coupling equations (4) to (15), the damping of the sample can be obtained at each maximum strain; for the whole temperature range of the test. In addition, the strength of ADD effects can be measured through S parameter, such that [23-26],

$$S = \frac{\Delta Q^{-1}{}_S}{\Delta \varepsilon_0} \tag{18}$$

The frequency during the free decaying of oscillations of the composite oscillator was calculated from the recorded decaying oscillation, see upper inset in Figure 2. Besides, the frequency (f) and wavelength (λ) for each one of the components satisfy the well-known relationship, $f \cdot \lambda = v$; where v is the speed of sound in each component. Thus, by knowing the speed of sound (or wavelength) of all elements of the oscillator, the elastic modulus, E, can be obtained from $\rho \cdot v^2 = E$; as it was explained above.

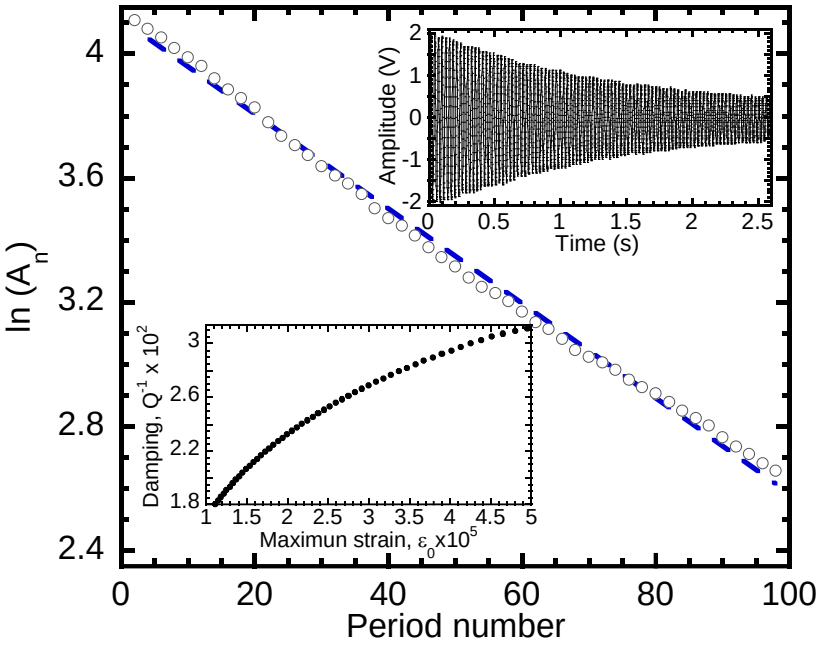

Figure 2: Logarithm of the decaying areas ($\ln(A_n)$) vs period number which presents non-linear effects (open circles). Dashed line represents the linear regression of the curve. Upper inset: oscillation decay. Lower inset: damping as a function of maximum strain on the sample obtained from equation (17).

In the case that the speed of sound is unknown, the changes which appears in the frequency of the whole oscillator can be used in order to infer the frequency changes which occurs in the sample as a consequence of the changes in the elastic modulus, see for more details Ref. [15].

Differential Thermal Analysis (DTA) measurements were carried out at a heating/cooling rate of 10K/min in a conventional calorimeter with stainless steel crucibles, under argon protective atmosphere at normal pressure.

Magnetic measurements were performed in a QD MPMS XL-7 SQUID magnetometer under constant applied magnetic fields of 100 Oe. Measurements were made on cooling–heating cycles at 1 K/min.

4. RESULTS AND DISCUSSION

DTA and SQUID measurements were performed in order to determine the MT temperature for three different compositions. Figures 3 show the thermal behaviour, after the base-line subtraction, and magnetic response for (a) Ti0, (b) Ti05 and (c) Ti2. As it can be seen from Figure 3, the MT temperatures for the three alloys, Ti0, Ti05 and Ti2, are 330 K, 340 K and 360 K, respectively. In addition, in Ti2 sample (see Figure 3(c)), it can be detected another process just below the MT temperature; which can be inferred by the appearance of both the peak in the SQUID spectrum and the hump in the low temperature tail in the DTA reaction peak.

In order to study the MT from the mechanical point of view, mechanical spectroscopy measurement has been also performed. Figures 4 show the temperature dependence of the damping and frequency for the three FSMA around the MT zone. The damping peak (Figure 4(a)) and the step down in the squared frequency (Figure 4(b)) (proportional to elastic modulus reveal that the MT for Ti0, Ti05 and Ti2 is around 335 K, 340 K and 345 K, respectively. These temperatures are in agreement with the temperatures obtained from SQUID and DTA, except for Ti2 where there appears a discrepancy in the MT temperatures among different techniques.

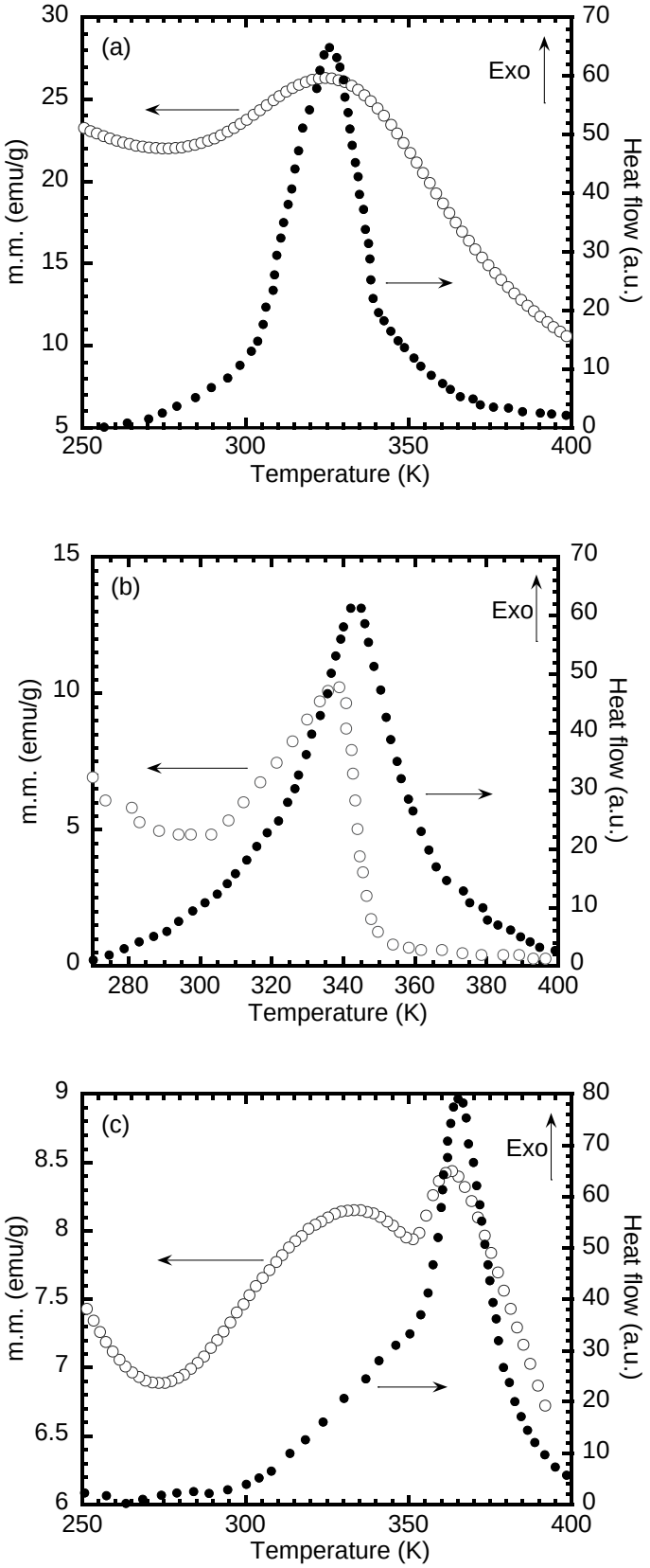

Figure 3: SQUID (open circles, left axis) and DTA (full circles, right axis) measurement as a function of temperature for the ferromagnetic shape memory alloys (a) Ti0, (b) Ti05 and (c) Ti2, around the MT.

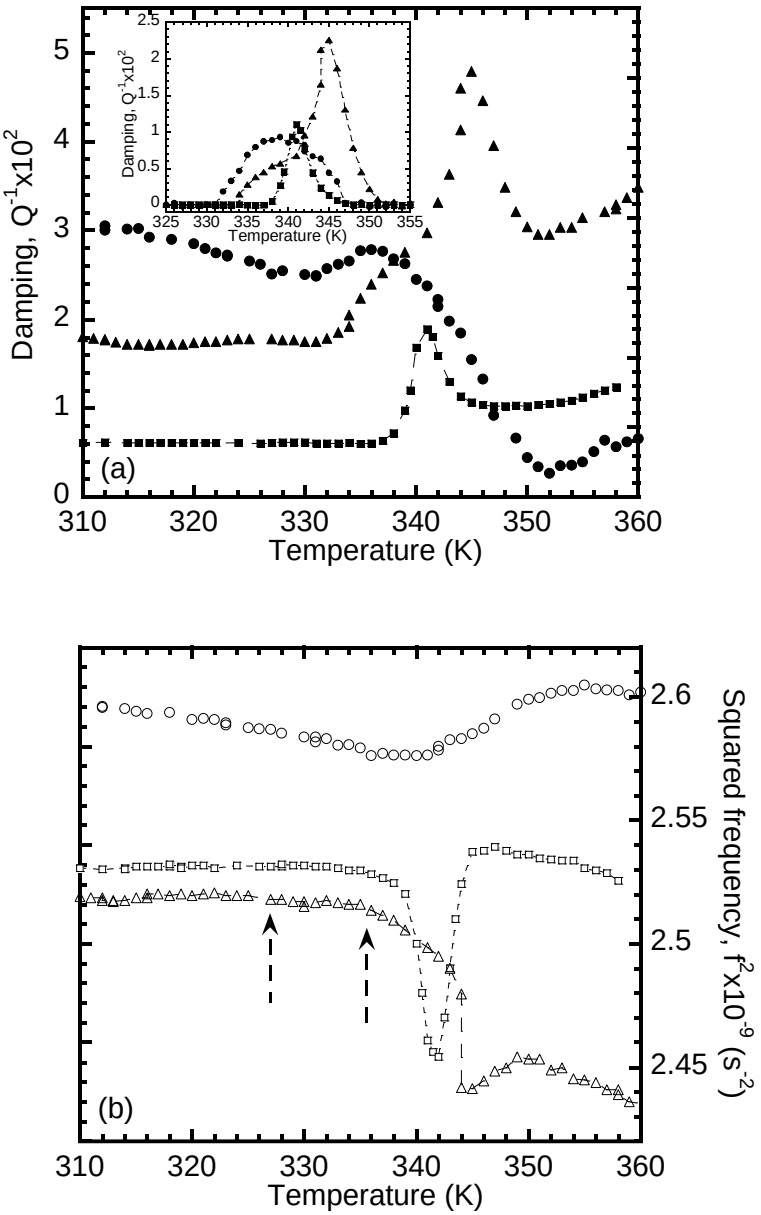

Figure 4: Damping (full symbols) and resonant frequency (empty symbols) curves as a function of temperature for the ferromagnetic shape memory alloys Ti0 (circles), Ti05 (squares) and Ti2 (triangles), around the martensitic transformation (MT). Dashed line is a guide for the eyes. Inset: MT damping peak after background subtraction for the three alloys.

It should be highlighted that, the main differences between the three alloys were: (i) the dependence of the MT temperature as a function of the concentration of titanium and (ii) the increase of the MT damping peak height (after background subtraction, see inset in the Figure 4(a)) as the concentration of titanium increases. In addition, another relaxation process seems to appear at around 365 K just above the MT in Ti0 sample. Moreover, different relaxation processes were also detected below MT temperature as a hump in the low temperature tail of the martensitic peak and by the two stage modulus change in Ti2 sample (see dashed arrows in Figure 4(b)). This behaviour is in agreement with both the peak in SQUID spectrum and the hump in DTA peak, and it could be related with the magnetic relaxation process. Besides, from the comparison of the damping curves, another remarkable difference in the shape of the spectrum can be also detected. In fact, the spectra of samples Ti05 and Ti2 exhibit damping values for the background in the martensite phase lower than in the austenite phase. This behaviour above MT temperature could be related with the damping values corresponding to a low temperature tail of a relaxation peak at higher temperatures. The behaviour of the squared frequency is in agreement with the beginning of the relaxation process. Measurement at higher

temperatures should be performed, but thermal treatment could deteriorate the memory effect by means of the decomposition of the matrix. In contrast, in sample Ti0, damping values for background in martensite phase are higher than in austenite phase. This latest case in the mechanical spectroscopy spectrum in FSMA is the expected usually.

In order to explore the movement of twin boundaries in NiMnSn alloy without doping, the appearance of ADD has been checked through the S parameter for Ti0 sample. Figure 5 shows the S values (see equation (18)) as a function of temperature for the damping spectrum corresponding of the Ti0 sample in Figure 4(a). The S values differ from zero for temperatures below MT, where the martensitic phase occurs. Non-linear anelasticity is selectively related to the motion of linear/planar defects and therefore is an efficient tool of studying pinning-related phenomena [17,23,27]. At higher temperatures than the MT temperature the S values become null, indicating the appearance non-linear effect in the martensite range. The ADD effect is related with the movement of the twin boundary and their interaction with defect as point defects or dislocations [17].

Figure 5 also shows the damping spectrum as a function of temperature for different maximum strain in the sample. Below the MT temperature, as higher the maximum strain in the sample, higher are the damping values.

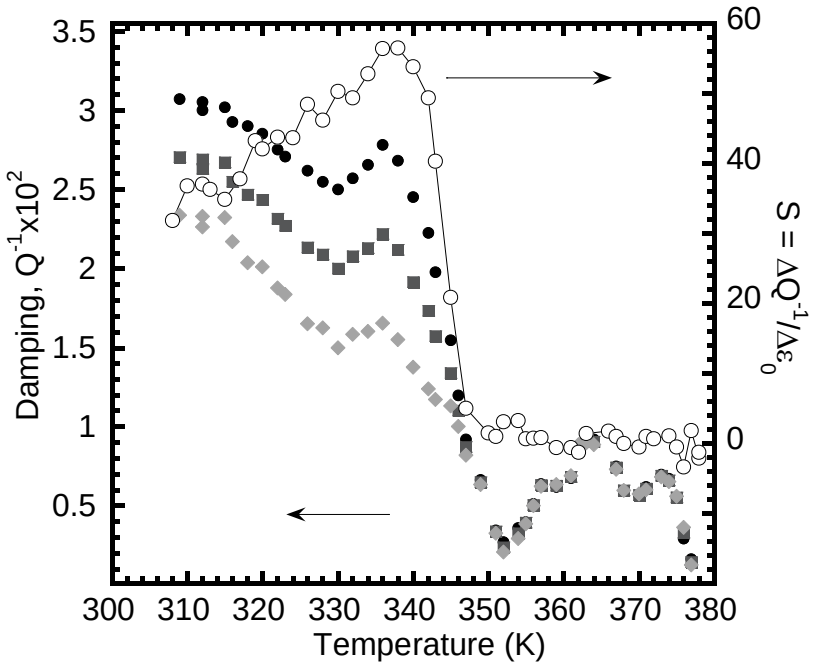

Figure 5: Amplitude dependent damping curves as a function of temperature in the zone of the martensitic phase (Circles: 5×10^{-5}, Squares: 4×10^{-5}, Rhombuses: 3.5×10^{-5}) and strength of the amplitude dependent damping ($S = \Delta Q^{-1}/\Delta\varepsilon_0$) for Ti0 alloy.

5. CONCLUSIONS

Mechanical spectroscopy measurements as a function of temperature and strain has been performed in NiMnSnTi ferromagnetic shape memory alloys, by means of a piezoelectric composite oscillator recently developed. This new equipment was a good solution to perform mechanical spectroscopy measurement in small and brittle samples.

An increase of both the martensitic transformation temperature and the martensitic transformation peak height with the addition of Ti has been detected. On the other hand, the damping spectra for samples Ti05 and Ti2 exhibit background values which are lower in the martensite phase than in the austenite one.

In Ti2 sample an additional relaxation process near the martensitic transition temperature has been observed. It is probably related to a magnetic relaxation process, as can be inferred from SQUID measurements. However, the values of MT temperatures obtained from the different techniques shows a discrepancy between MS, DTA and SQUID. In fact, this discrepancy could be promoted by the appearance of micro-pores into these samples, generating zones with internal stresses and/or micro-cracks which are

more sensitive to MS tests, than thermal/magnetic measurements. It highlights the requirement to evaluate the MT temperature through different techniques.

The appearance of non-linear damping as a function of the oscillating strain has been detected in the martenistic range for all the studied alloys by means of S parameter.

6. ACKNOWLEDGMENTS

This work has been carried out with the financial support of the CONICET-PIP 2098 and 0179, and the PID-UNR; ING 453 (2014-2017). Authors also wish to acknowledge to the Cooperation Agreement between the Universidad Pública de Navarra and the Universidad Nacional de Rosario, Res. 5789/2013 and Res. 3247/2015, and Universidad del País Vasco and the Universidad Nacional de Rosario, Res. CS.788/89 – 1792/2003, UPV224.310-14553/02, Res. 3469/2007, Res. CS. 124/2010 and Res. 3243/2015.

7. BIBLIOGRAPHY

[1] ULLAKKO, K., HUANG, J.K., KANTNER, R.C., *et al*., "Large magnetic-field-induced strains in Ni2MnGa single crystals", *Applied Physics Letters*, v. 69, n. 13, pp. 1966-1968, 1996.

[2] KRENKE, T., DUMAN, E., ACET, M., *et al*., "Inverse magnetocaloric effect in ferromagnetic Ni–Mn–Sn alloys", *Nature materials*, v. 4, n. 6, pp. 450-454, 2005.

[3] PLANES, A., MAÑOSA, L., ACET, M., "Magnetocaloric effect and its relation to shape-memory properties in ferromagnetic Heusler alloys", *Journal of Physics: Condensed Matter*, v. 21, n. 23, pp. 233201, 2009.

[4] WEBSTER, P.J., ZIEBECK, K.R.A., TOWN, S.L., *et a*l., "Magnetic order and phase transformation in Ni2MnGa", *Philosophical Magazine B*, v. 49, n. 3, pp. 295-310, 1984.

[5] KRENKE, T., ACET, M., WASSERMANN, E.F., *et al*., "Martensitic transitions and the nature of ferromagnetism in the austenitic and martensitic states of Ni− Mn− Sn alloys", *Physical Review B*, v. 72, n. 1, pp. 014412, 2005.

[6] KRENKE, T., ACET, M., WASSERMANN, E.F., *et al*., "Ferromagnetism in the austenitic and martensitic states of Ni− Mn− In alloys", *Physical Review B*, v. 73, n. 17, pp. 174413, 2006.

[7] AKSOY, S., ACET, M., DEEN, P.P., *et a.l*, "Magnetic correlations in martensitic Ni-Mn-based Heusler shape-memory alloys: Neutron polarization analysis", *Physical Review B*, v. 79, n. 21, pp. 212401, 2009.

[8] KAINUMA, R., IMANO, Y., ITO, W., *et al.*, "Magnetic-field-induced shape recovery by reverse phase transformation", *Nature*, v. 439, n. 7079, pp. 957-960, 2006.

[9] ITO, W., ITO, K., UMETSU, R.Y., KAINUMA, R., *et al*., "Kinetic arrest of martensitic transformation in the NiCoMnIn metamagnetic shape memory alloy", *Applied Physics Letters*, v. 92, n. 2, pp. 21908-21908, 2008.

[10] PÉREZ-LANDAZÁBAL, J.I., RECARTE, V., SÁNCHEZ-ALARCOS, V., *et al.*, "Magnetic field induced martensitic transformation linked to the arrested austenite in a Ni-Mn-In-Co shape memory alloy", *Journal of Applied Physics*, v. 109, n. 9, pp. 093515, 2011.

[11] PÉREZ-LANDAZÁBAL, J.I., RECARTE, V., SÁNCHEZ-ALARCOS, *et al*., "Effect of magnetic field on the isothermal transformation of a Ni–Mn–In–Co magnetic shape memory alloy", *Intermetallics*, v. 28, pp. 144-148, 2012.

[12] BUDRUK, A., PHATAK, C., PETFORD-LONG, A.K., *et al*., "In situ Lorentz TEM magnetization studies on a Fe–Pd–Co martensitic alloy", *Acta Materialia*, v. 59, n. 17, pp. 6646-6657, 2011.

[13] PÉREZ-LANDAZÁBAL, J.I., LAMBRI, O.A., BONIFACICH, F.G., *et al*., "Influence of defects on the irreversible phase transition in Fe–Pd ferromagnetic shape memory alloys", *Acta Materialia*, v. 86, pp. 110-117, 2015.

[14] BONIFACICH, F.G., LAMBRI, O.A., PÉREZ-LANDAZÁBAL, J.I., *et al*., "Mobility of Twin Boundaries in Fe-Pd-Based Ferromagnetic Shape Memory Alloys", *Materials Transactions, JIM*, v. 57, n. 10, pp. 1837-1844, 2016.

[15] BONIFACICH, F.G., LAMBRI, O.A., PÉREZ-LANDAZÁBAL, J.I., *et al*., "Piezoelectric composite oscillator for measuring mechanical spectroscopy in small samples that non-match in half wavelength", *Measurement Science and Technology*, v. 27, n. 3, pp. 035902, 2016.

[16] MARX, J., "Use of the piezoelectric gauge for internal friction measurements", *Review of Scientific In-*

struments, v. 22, n. 7, pp. 503-509, 1951.

[17] SCHALLER, R., FANTOZZI, G., GREMAUD. G. (eds.), *Mechanical Spectroscopy*. Switzerland, Trans. Tech. Publ. Ltd, 2001.

[18] NOWICK, A.S., BERRY, B.S. *Anelastic relaxation in crystalline solids*. New York, USA, Academic Press, 1972.

[19] ROBINSON, W.H., EDGAR, A., "The piezoelectric method of determining mechanical damping at frequencies of 30 to 200 kHz", *IEEE Transactions on Sonics and Ultrasonics*, v. 21, n. 2, pp. 98-105, 1974.

[20] DEVINE, S.D., ROBINSON, W.H., "Piezoelectric method of determining mechanical properties of a small sandwich specimen at 30 to 200 kHz", *Journal of Applied Physics*, v. 48, n. 4, pp. 1437-1441, 1977.

[21] DEVINE, S.D., ROBINSON, W.H., COLLINS, M.A., "Effect of strain on the ESR parameters for tetragonal Gd 3+ in CaF 2 using ultrasonic modulation", *Journal of Magnetic Resonance*, v, 13, n. 1, pp. 1-10, 1974.

[22] KITTEL, C., *Introduction to Solid State Physics*, New York, USA, John Wiley & Sons Inc., 1996.

[23] LAMBRI, O.A. "A review on the problem of measuring nonlinear damping and the obtainment of intrinsic damping", In: Martinez-Mardones, J., Walgraef, D., Wörner, C.H. (eds.). *Materials Instabilities*. New York, USA, World Scientific Publishing Co Pte Ltd, 2000.

[24] MOLINAS, B.J., LAMBRI, O.A., WELLER, M., "Study of non-linear effects related to the Snoek-Köster relaxation in Nb", *Journal of alloys and compounds*, v. 211, pp. 181-184, 1994.

[25] ZELADA-LAMBRI, G.I., LAMBRI, O.A., GARCÍA, J.A., "Mechanical energy losses due to the movement of dislocations in molybdenum at high temperatures (0.3T m)", *Journal of nuclear materials*, v. 353, n. 1, pp. 127-134, 2006.

[26] MOLINAS, B.J., POVOLO, F., "Analysis of the problem of converting measured amplitude-dependent internal friction to intrinsic values. Detailed study of the case of forced oscillations", *Journal of Physics E: Scientific Instruments*, v. 20, n. 8, pp. 970, 1987.

[27] BATIST, R. "Mechanical spectroscopy", In: Lifshin, E. (ed.). "Characterization of Materials", In: Cahn, R.W., Haasen, P., Kramer, E.J. (eds.), *Materials Science and Technology*, v. 2B, Part II, Weinheim, VCH, 1991.